ACS OMEGA

Article

Cite This: ACS Omega 2020, 5, 1634−1639

Rendering Redox Reactions of Cathodes in Li-Ion Capacitors Enabled by Lanthanides

Kaiqiang Zhang,[†,‡] Tae Hyung Lee,[†] Mohammad A. Khalilzadeh,[§] Rajender S. Varma,[*,∥] Ji-Won Choi,[*,‡] Ho Won Jang,[*,†] and Mohammadreza Shokouhimehr[*,†]

[†]Department of Materials Science and Engineering, Research Institute of Advanced Materials, Seoul National University, Seoul 08826, Republic of Korea

[‡]Electronic Materials Center, Korea Institute of Science and Technology (KIST), Seoul 136-791, Republic of Korea

[§]Department of Forest Biomaterials, College of Natural Resources, North Carolina State University, Raleigh, North Carolina 27607, United States

[∥]Regional Center of Advanced Technologies and Materials, Department of Physical Chemistry, Faculty of Science, Palacky University, Šlechtitelů 27, 783 71 Olomouc, Czech Republic

Supporting Information

ABSTRACT: Capacitors allow extremely fast charge and discharge operations, which is a challenge faced by recent metal-ion batteries despite having highly improved energy densities. Thus, combined type electric energy storage devices that can integrate high energy density and high power density with high potentials, can overcome the shortcomings of the current metal-ion batteries and capacitors. However, the limited capacities of cathode materials owing to the barren redox reactions are regarded as an obstacle for the development of future high-performance hybrid metal-ion capacitors. In this study, we demonstrate the redox-reaction-rendering effect of the much overlooked lanthanide elements when used as the cathode of lithium-ion capacitors using the mesoporous carbon (MC) as a matrix material. Consequently, these lanthanide elements can effectively enrich the redox reaction, thus improving the capacity of the matrix materials by more than two times. Typically, the Gd-elemental decoration of MC surprisingly enhances the capacity by almost two times as compared with the underacted MC. Furthermore, the La nanoparticles (NPs) decoration depicts the same behavior. Evident redox peaks were formed on the original rectangular cyclic voltammetry (CV) curves. This study provides the first example of embedding lanthanide elements on matrix materials to enrich the desired redox reactions for improving the electrochemical performances.

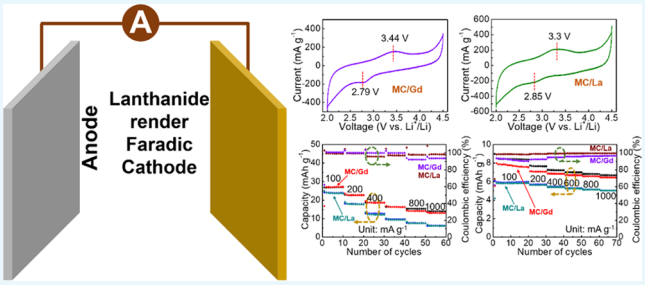

INTRODUCTION

The integration of renewable- and sustainable-energy resources into electric grids is considered as a promising approach for solving the energy crisis caused by the limited quantities of fossil fuels.[1−4] However, intermediate energy-storage devices are required for balancing and stabilizing green energy due to its instability.[5−11] Electrochemical batteries exhibit a significant potential to assist in this crucial coupling operation. Thus far, there have been extensive advancements in lithium-ion batteries (LIBs) as compared to other parallel metal−ion batteries.[12−20] However, there are still a few challenges associated with the use of LIBs, namely, the unmatched energy and power densities. The energy densities of LIBs have been highly improved using diverse design strategies for anode and cathode materials.[21−23] However, the power densities of LIBs are still limited due to the poor electronic and ionic conductivities of the active materials. Capacitors are suitable to meet high power density requirements and overcome these challenges. However, traditional capacitors function on charge gathering and releasing, thereby limiting the capacitances. These aspects of metal-ion batteries and capacitors indicate that they can provide a solution for each other's limitations and address the current electronic-energy storage issues.

Hybrid capacitors constructed using battery-type anodes and capacitor-type cathodes gradually achieve a promising combination of both high energy and power densities. The current researches on this type of electronic storage devices mainly focus on the exploration of anode materials to achieve both high capacities and rate performances.[24−26] Most of the current cathode material used in hybrid capacitors is activated carbon, although other types of functionalized carbon-based materials have also been reported.[27,28] Mesoporous carbon (MC) is one of the highly porous and cost-efficient materials, and it is, in principle, quite suitable as a cathode material in

Received: November 1, 2019
Accepted: December 4, 2019
Published: January 15, 2020

DOI: 10.1021/acsomega.9b03699
ACS Omega 2020, 5, 1634−1639

hybrid capacitors. However, bare MC materials endow very limited capacitances. Therefore, the further engineering of mesoporous is necessary to have more redox-active sites for achieving Faradic pseudocapacitance. The introduction of redox reactions requires alterable valance states to integrate foreign electrons and ions.

Accordingly, lanthanide elements have rich unpaired electrons and special orbital structures, along with the capabilities of multiple valances. Among these elements, gadolinium (Gd) has seven unpaired electrons in the 4f orbital and one unpaired electron in the 6p orbital. On the contrary, lanthanum (La) has a single unpaired electron in the 6p orbital. Their salts are well soluble and stable trivalent-ion states in the solution. Based on our previously conducted report,[29] the Gd-based Prussian-blue analogue contributes to highly improved capacity for Li-ion capacitors as compared to other carbon-based cathode materials for hybrid capacitors. Motivated by these advantages of often-overlooked lanthanide elements, in this study, we demonstrated the lanthanide elements rendered redox reactions for MC when used as cathode materials in hybrid lithium-ion capacitors. Typically, we doped Gd and La on the MC via a wet-chemical method using the water-soluble reductant $NaBH_4$.[30−32] As a result, the desired redox peaks were generated clearly on cyclic voltammetry (CV) curves. By deriving benefits from both the effective redox reactions of lanthanide elements and the capacitive-type Li^+-ion storage property of mesoporous C, three times enhancement in the capacity values is achieved, along with an extremely long cyclic stability, as compared with that of the bare mesoporous C.

RESULTS AND DISCUSSION

The CV measurement of the MC was performed (Figure 1). A rectangular CV curve with a single redox peak at 3.44 V vs Li^+/Li in the charging process illustrates the capacitive Li^+-ion-storage mechanism in the voltage range of 2 V vs Li^+/Li. Correspondingly, the repeated charge−discharge measurement indicates the capacity values of approximately 8 mAh/g with excellent Coulombic efficiencies approaching 100%. The unit of capacity here is identified as that of the electrodes used for batteries rather than that of double-layer super capacitors or of Faradic pseudocapacitors. The linear charge−discharge voltage profiles in Figure S1 illustrate the capacitive Li^+-ion-storage process. In addition, the consecutive evolution of the voltage profiles is depicted in Figure S2, in which, steady charge and discharge processes are illustrated.

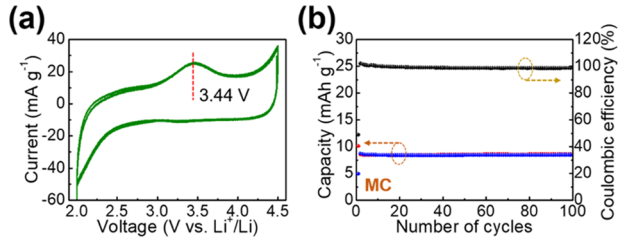

Figure 1. (a) CV curve and (b) repeated charge−discharge cycling measurements of bare mesoporous C used as the cathode of lithium-ion capacitor.

Furthermore, we enhance the capacities of MC by decorating the lanthanide elements (Gd and La). From the results of X-ray diffraction (XRD) phase identification (Figures 2a,d and S3a), the absence of both Gd and La metallic or oxide peaks suggests the small particle sizes of the loaded species. Furthermore, the D band and the G band from the MC component are identified from its Raman spectra (Figure 2b,e). The D band (A_{1g} mode) and the G band (E_{2g} mode) reveal both amorphous and crystalline carbon atoms, which is similar to the bare MC (Figure S3b). These results further suggest that the introduction of lanthanide elements has slight effect on the MC matrix. From the thermogravimetric analysis (TGA) results (Figures 2c,f and S3c), stable thermal plateaus are achieved for both the products after the initial evaporation of water molecules. Furthermore, the MC/Gd shows a greater amount of residual water species than that in MC/La. The stable thermal stability (Figure S3c) in the bare MC sample further suggests the introduced water molecules after synthesis process.

Subsequently, the small MC/Gd and MC/La particles were observed using scanning electron microscopy (SEM) and transmission electron microscopy (TEM) (Figure 3). Similar small composite particles are shown in SEM and TEM images (Figure 3a,e). The particle size measured from the TEM images (Figure 3b,f) was approximately 50 nm. The Gd or La is decorated on the MC, as determined from the energy-dispersive X-ray (EDX) mapping results (Figure 3c,d,g,h). Furthermore, Gd and La were loaded uniformly on the MC because of the reductant $NaBH_4$ by taking the benefit of surfactant cetyltrimethyl ammonium bromide (CTAB).

The loaded Gd and La are further demonstrated by the X-ray photoelectron spectra (XPS), in which the C species is clearly shown in the wide survey and the deconvoluted spectra (Figure 4a,b,e,f). The intense O 1s signal is released mainly from the absorbed water molecules. The successful loading of La on MC is confirmed by the intense deconvoluted La 3d peaks at the binding energies of 834 and 851 eV in the MC/La sample.[33] Furthermore, for the Gd in MC/Gd, a big hump is obtained, which only preliminarily confirms the existence of Gd but not the existing states.

Our aim is to improve the capacity values of the MC by the decoration or introduction of lanthanide elements. Thus, the CV curves are scanned, in which, a pair of redox peaks are clearly formed on both the CV curves (Figure 5). A reduction peak at 2.79 V vs Li^+/Li and an oxidation peak at 3.44 V vs Li^+/Li, with a hysteresis-voltage range of 0.65 V vs Li^+/Li, are exhibited for MC/Gd. However, for MC/La, a reduction peak at 2.85 V vs Li^+/Li and an oxidation peak at 3.3 V vs Li^+/Li with a narrower hysteresis voltage window of 0.45 V vs Li^+/Li are exhibited. After the decoration of these two lanthanide elements, an additive redox process is introduced in the MC, thereby expecting to modify the electrochemical capacity toward Li^+-ion storage.

The electrochemical capacity values are measured using multiple strategies (Figure 6). From the rate-performance results, a highly improved Li^+-ion-storage capability is obtained, with electrochemical capacities of approximately 25 and 28 mAh/g for MC/La and MC/Gd, respectively, at 100 mA/g, both of which are much higher than those of bare MC (9 mAh/g) (Figure 6a). Furthermore, excellent Coulombic efficiencies are obtained for both MC/Gd and MC/La at various current densities. A higher capacity retention of 53% for MC/Gd and 26% for MC/La are also obtained after enhancing the current density to 1000 mA/g. This can be further explained by the electrochemical-impedance measurements (Figure S4a,b). Furthermore, the electrochemical

DOI: 10.1021/acsomega.9b03699
ACS Omega 2020, 5, 1634−1639

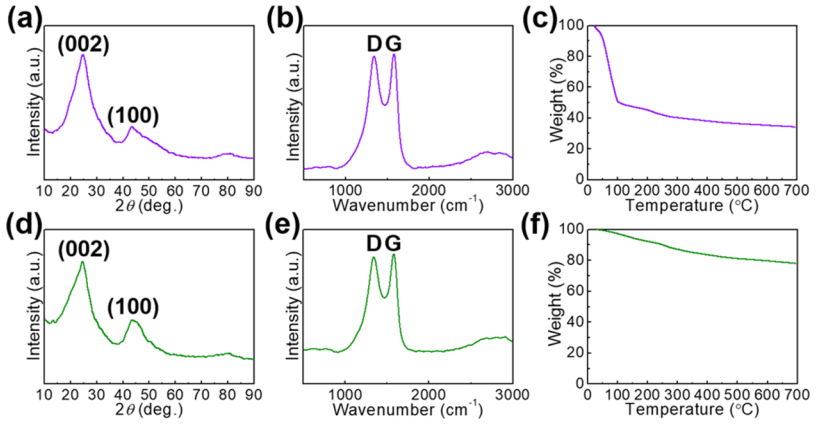

Figure 2. XRD patterns of (a) MC/Gd and (d) MC/La. Raman spectra of (b) MC/Gd and (e) MC/La. TGA curves of (c) MC/Gd and (f) MC/La.

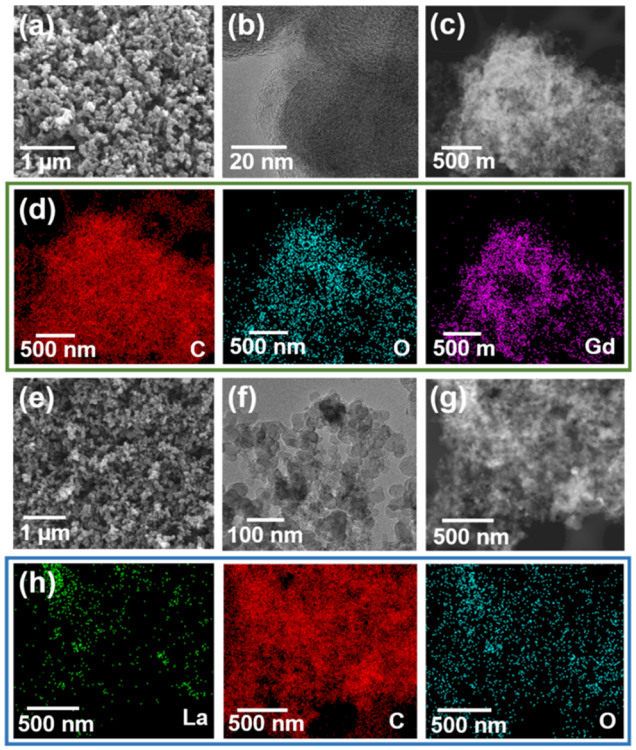

Figure 3. SEM images of (a) MC/Gd and (e) MC/La. TEM images of (b) MC/Gd and (f) MC/La. Scanning transmission electron microscopy (STEM) images of (c) MC/Gd and (g) MC/La. EDX mapping of (d) MC/Gd and (h) MC/La.

impedance spectroscopy (EIS) curves depict a depressed semicircle (charge transfer) and an oblique line (mass transfer).[34,35] The EIS curves were further analyzed by incorporating a corresponding equivalent circuit (Figure S4c). In these, the internal resistance (R_s ~ 50 Ω) corresponding to the electrode resistance, electrolyte resistance, electrode/current collector contact resistance, and current-collector resistance are depicted. As a sequence, charge-transfer resistances (R_{ct}) of approximately 200 Ω for MC/Gd and 400 Ω for MC/La are also depicted. The underlying charge−discharge voltage profiles are recorded in Figure 6c,d, in which a pair of evident voltage plateaus is displayed at approximately 3.5 V vs Li^+/Li upon increasing the current density from 100 to 1000 mA/g. These results highly suggest the rendering effect toward the redox reactions using the lanthanide elements to effectively promote the electrochemical performances. Afterward, a more realistic consideration has been provided. In the practical utilization, one-time fast charge for a long-term application is crucial, making it necessary to demonstrate the cathode materials in a manner of fast charge and discharge at various current densities. Thus, based on the corresponding results in Figure 6b, the capacity values of approximately 8 mAh/g for MC/Gd and 6 mAh/g for MC/La, both at 100 mA/g, are retained. Meanwhile, the capacity values of 7 mAh/g for MC/Gd and 5 mAh/g for MC/La are retained after increasing the current density up to 1000 mA/g with Coulombic efficiencies of both approaching 100%. Furthermore, the consecutive charge−discharge measurements are performed at 100 mA/g for both MC/Gd and MC/La. The highly improved capacities are steadily maintained (25 mAh/g for MC/Gd and 20 mAh/g for MC/La at the 100th cycle) with excellent Coulombic efficiencies of both approaching 100% (Figure S5).

Long-term application is significant for the cathode materials used in practical devices. We, therefore, measure the long-term, repeated charge−discharge cycling at both 1000 and 10 000 mA/g (Figure 6e,f). As a result, it exhibits quite stable long-term charge/discharge performances.

After consecutive charge−discharge measurements, we further investigated the electrodes. A similar electrode morphology having a highly porous structure was exhibited. Furthermore, the decorated nanoparticles on the MC were observed in the TEM images (Figure S6). This observation confirmed the well integrity of the composite materials, together with the EDX mapping results in Figure S7 in which the elements were detected satisfactorily.

CONCLUSIONS

In this work, we demonstrated the redox reaction rendering by introducing lanthanide elements. The MC was employed as a reference and host/support material. After the decoration of lanthanide elements via a facile wet-chemical method, together with using CTAB as a surfactant, even the slightly small sized particles Gd and La particles could be loaded on the MC. Meanwhile, these lanthanide elements could also effectively enrich the redox reaction, thus improving the capacity of the matrix materials. Typically, the Gd-elemental decoration of MC surprisingly enhanced the capacity by almost two times than that of the bare MC. In addition, the La nanoparticles

DOI: 10.1021/acsomega.9b03699
ACS Omega 2020, 5, 1634−1639

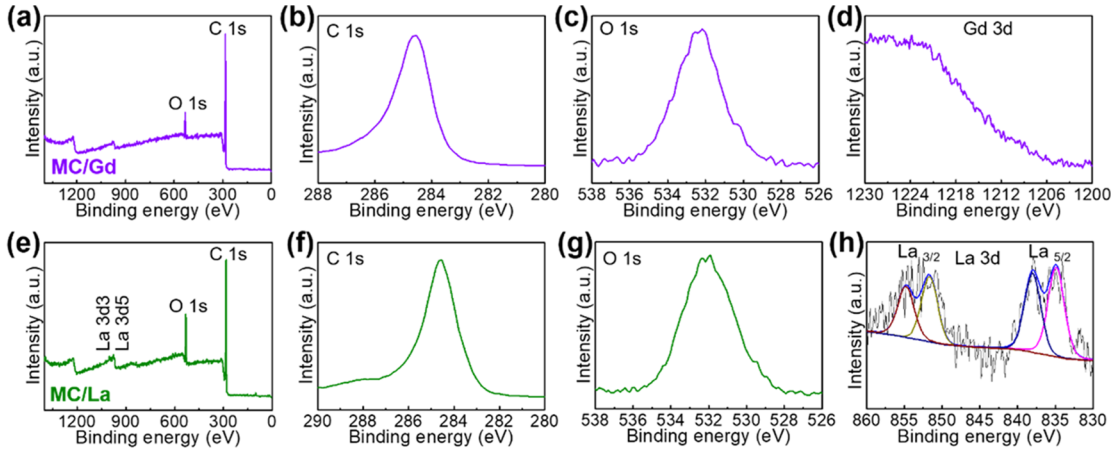

Figure 4. XPS spectra of MC/Gd: (a) wide survey, (b) C 1s, (c) O 1s, and (d) Gd 3d. XPS spectra of MC/La: (e) wide survey, (f) C 1s, (g) O 1s, and (h) La 3d.

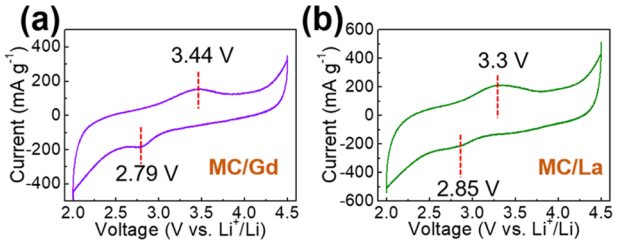

Figure 5. CV curves of (a) MC/Gd and (b) MC/La as a cathode material of lithium-ion capacitors.

(NPs) decoration depicted the same behavior. This study provides the first example of embedding lanthanide elements on matrix materials to render the desired redox reactions, for improving the electrochemical performances.

EXPERIMENTAL SECTION

Material Preparation. First, 0.5 g of MC (699632-5G, 0.342 cm^3/g (pore size), 150−250 m^2/g (surface area)), and 0.1 g of cetyltrimethyl ammonium bromide (CTAB, 219374-100GM) were dissolved in a 30 mL aqueous solution containing 10 mL ethanol additive, followed by ultrasonication. CTAB is an efficient surfactant that can provide a mild environment for the nanoparticle loading. Subsequently, 0.01 moles each of gadolinium (III) nitrate hexahydrate (211591-25G) and lanthanum (III) nitrate hexahydrate (203548-25G) were dissolved separately in 10 mL of aqueous solutions. After the ultrasonication of both solutions for 1 h, we mixed the lanthanide-element containing solutions separately into the previously prepared MC solution, followed by constant stirring. Following this, a 0.2 M $NaBH_4$ solution was added to it. $NaBH_4$ is a low-cost and widely used reductant that provides sufficient reductant agent. After the $NaBH_4$ (71320-25G)-induced reduction process, the suspended species were rinsed using copious amount of water and dried in an oven at 60 °C.

Characterizations. *Physical Characterizations.* The phases were studied by means of X-ray diffraction (XRD) using a Bruker D8 ADVANCE diffractometer. The surface chemical performances of the final products were determined using X-ray photoelectron spectroscopy (XPS) with an Al Kα source (PHI 5000 VersaProbe, Japan). Furthermore, Raman spectra were gathered using LabRAM HR Evolution and

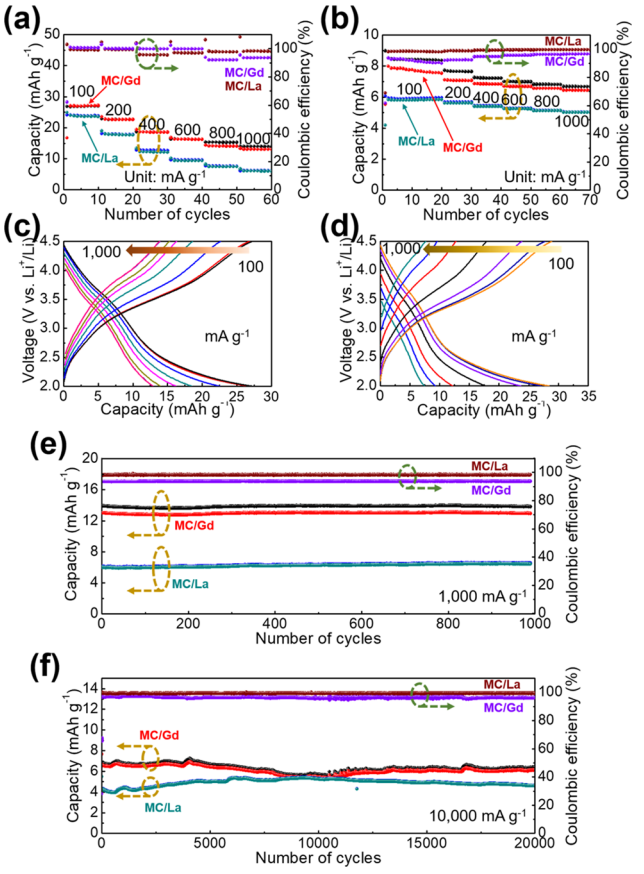

Figure 6. (a) Rate performances of MC/Gd and MC/La at various current densities (100, 200, 400, 600, 800, and 1000 mA/g). (b) Rate properties of MC/Gd and MC/La at the constant current density of 1000 mA/g for fast charging and diverse discharge current densities of 100, 200, 400, 600, 800, and 1000 mA/g. Charge−discharge voltage profiles of (c) MC/Gd and (d) MC/La at different current densities. Repeated charge−discharge of the products at the current densities of (e) 1000 mA/g and (f) 10 000 mA/g.

Nicolet iS50. Field emission scanning electron microscopy (FE-SEM, SUPRA 55VP) was utilized for verifying the compositions and morphologies of the synthesized samples. Transmission electron microscopy connected with an energy-dispersive X-ray spectrometer (TEM, JEOL JEM-F200) was

DOI: 10.1021/acsomega.9b03699
ACS Omega 2020, 5, 1634−1639

performed for studying decoration and morphology. The thermal stability of the as-prepared GdHCCo was probed by means of thermogravimetric analysis (TGA) at the rate of 10 °C/min from 25 to 700 °C under an N_2-flow condition. Furthermore, quantitative elemental analysis was achieved by means of X-ray fluorescence (XRF, ZSX-PRIMUS).

Electrode Preparation. A slurry was prepared by mixing and grinding the bare MC, carbon black (Super P Li), and poly(vinylidene difluoride) in the weight ratio of 7:2:1. Subsequently, the mixed powder was dried for 8 h at 80 °C in a vacuum oven, followed by redispersing it into *N*-methyl-2-pyrrolidinone. The weight of samples was measured before and after the drying to ensure the water evaporation as much as possible. A working electrode was prepared using a loading amount of approximately 3 mg/cm^2 on an Al-foil current collector by spreading the slurry and, subsequently, drying it in a vacuum oven at 60 °C. Similar methods were also used for preparing the electrodes that contained MC/Gd and MC/La products by only changing the MC into MC/Gd and MC/La, respectively.

Electrochemical Characterization. A two-electrode-type cell comprising the working electrode as an MC or MC/Gd or MC/La, and sufficient Li-metal foil to ensure that capacity was restricted only by the product materials, was prepared in a 1.0 M mixture of $LiPF_6$ with diethylene carbonate and ethylene carbonate (1:1, v/v) in an Ar-filled glovebox. The redox activities were determined by means of CV curves using an electrochemical workstation (WBCS3000, Wonatech, Korea). The employed potential range was 2.2−4.5 V vs Li^+/Li at the rate of 0.5 mV/s. In addition, the galvanostatic charge/discharge was achieved between the same potential range of 2.2−4.5 V vs Li^+/Li under various specific currents of 100, 200, 400, 600, 800, 1000, and 10 000 mA/g. The all-specific capacities and current densities were calculated on the basis of the total weight of MC or MC/Gd or MC/La. Furthermore, the electrochemical-impedance-spectroscopy (EIS) measurements (IM6ex ZAHNER Elektrik) were performed at a frequency range of 10 mHz to 1 MHz under an amplitude of 10 mV.

Ex Situ Characterizations. Ex situ characterizations were performed to investigate the decorated Gd and La elements after cycling measurements. The measured half-cells were disassembled, followed by thoroughly rinsing the working electrode materials in an Ar-filled glovebox. After being vacuum dried for 8 h, the electrode materials were subjected to ex situ TEM and SEM characterizations.

■ ASSOCIATED CONTENT

Supporting Information

The Supporting Information is available free of charge at https://pubs.acs.org/doi/10.1021/acsomega.9b03699.

Electrochemical measurement of bare MC; voltage profiles of the bare MC; EIS curves; repeated charge−discharge operations; SEM and TEM images; and STEM and EDX mapping images (PDF)

■ AUTHOR INFORMATION

Corresponding Authors

*E-mail: varma.rajender@epa.gov (R.S.V.).
*E-mail: jwchoi@kist.re.kr (J.-W.C.).
*E-mail: hwjang@snu.ac.kr (H.W.J.).
*E-mail: mrsh2@snu.ac.kr, shokouhimehrm@gmail.com (M.S.).

ORCID

Rajender S. Varma: 0000-0001-9731-6228
Ji-Won Choi: 0000-0002-7701-3227
Ho Won Jang: 0000-0002-6952-7359
Mohammadreza Shokouhimehr: 0000-0003-1416-6805

Notes

The authors declare no competing financial interest.

■ ACKNOWLEDGMENTS

This research was supported by Korea Institute of Science and Technology Future Resource Program (2E29400). Furthermore, the financial supports of the Future Material Discovery Program (2016M3D1A1027666), the Basic Science Research Program (2017R1A2B3009135) through the National Research Foundation of Korea, and China Scholarship Council (201808260042) are appreciated.

■ REFERENCES

(1) Zhang, K.; Lee, T. H.; Cha, J. H.; Varma, R. S.; Choi, J.-W.; Jang, H. W.; Shokouhimehr, M. Two-dimensional boron nitride as a sulfur fixer for high performance rechargeable aluminum-sulfur batteries. *Sci. Rep.* **2019**, *9*, No. 13573.

(2) Zhang, K.; Lee, T. H.; Cha, J. H.; Jang, H. W.; Choi, J.-W.; Mahmoudi, M.; Shokouhimehr, M. Metal-organic framework-derived metal oxide nanoparticles@reduced graphene oxide composites as cathode materials for rechargeable aluminium-ion batteries. *Sci. Rep.* **2019**, *9*, No. 13739.

(3) An, W.; Gao, B.; Mei, S.; Xiang, B.; Fu, J.; Wang, L.; Zhang, Q.; Chu, P. K.; Huo, K. Scalable synthesis of ant-nest-like bulk porous silicon for high-performance lithium-ion battery anodes. *Nat. Commun.* **2019**, *10*, No. 1447.

(4) Han, J.-G.; Kim, K.; Lee, Y.; Choi, N.-S. Scavenging materials to stabilize $LiPF_6$-containing carbonate-based electrolytes for Li-ion batteries. *Adv. Mater.* **2019**, *31*, No. 1804822.

(5) Zhang, K.; Lee, T. H.; Jang, H. W.; Shokouhimehr, M.; Choi, J.-W. A hybrid energy storage mechanism of zinc hexacyanocobaltate-based metal-organic framework endowing stationary and high-performance lithium-ion storage. *Electron Mater. Lett.* **2019**, *15*, 444−453.

(6) Zhang, K.; Varma, R. S.; Jang, H. W.; Choi, J.-W.; Shokouhimehr, M. Iron hexacyanocobaltate metal-organic framework: highly reversible and stationary electrode material with rich borders for lithium-ion batteries. *J. Alloys Compd.* **2019**, *791*, 911−917.

(7) Zhang, K.; Lee, T. H.; Bubach, B.; Ostadhassan, M.; Jang, H. W.; Choi, J.-W.; Shokouhimehr, M. Coordinating gallium hexacyanocobaltate: Prussian blue-based nanomaterial for Li-ion storage. *RSC Adv.* **2019**, *9*, 26668−26675.

(8) Zhang, K.; Lee, T. H.; Bubach, B.; Ostadhassan, M.; Jang, H. W.; Choi, J.-W.; Shokouhimehr, M. Layered metal-organic framework based on tetracyanonickelate as a cathode material for in situ Li-ion storage. *RSC Adv.* **2019**, *9*, 21363−21370.

(9) Zhu, G.; Ma, L.; Lin, H.; Zhao, P.; Wang, L.; Hu, Y.; Chen, R.; Chen, T.; Wang, Y.; Tie, Z.; Jin, Z. High-performance Li-ion capacitor based on black-TiO_{2-x}/graphene aerogel anode and biomass-derived microporous carbon cathode. *Nano Res.* **2019**, *12*, 1713−1719.

(10) Zhu, G.; Chen, T.; Wang, L.; Ma, L.; Hu, Y.; Chen, R.; Wang, Y.; Wang, C.; Yan, W.; Tie, Z.; Liu, J.; Jin, Z. High energy density hybrid lithium-ion capacitor enabled by Co_3ZnC@N-doped carbon nanopolyhedra anode and microporous carbon cathode. *Energy Storage Mater.* **2018**, *14*, 246−252.

(11) Chen, T.; Cheng, B.; Chen, R.; Hu, Y.; Lv, H.; Zhu, G.; Wang, Y.; Ma, L.; Liang, J.; Tie, Z.; Jin, Z.; Liu, J. Hierarchical ternary carbide nanoparticle/carbon nanotube-inserted N-doped carbon

DOI: 10.1021/acsomega.9b03699
ACS Omega 2020, 5, 1634−1639

concave-polyhedrons for efficient lithium and sodium storage. *ACS Appl. Mater. Interfaces* **2016**, *8*, 26834−26841.
(12) Wang, B.; Ryu, J.; Choi, S.; Zhang, X.; Pribat, D.; Li, X.; Zhi, L.; Park, S.; Ruoff, R. S. Ultrafast-charging silicon-based coral-like network anodes for lithium-ion batteries with high energy and power densities. *ACS Nano* **2019**, *13*, 2307−2315.
(13) Wu, Y.; Wang, W.; Ming, J.; Li, M.; Xie, L.; He, X.; Wang, J.; Liang, S.; Wu, Y. An exploration of new energy storage system: high energy density, high safety, and fast charging lithium ion battery. *Adv. Funct. Mater.* **2019**, *29*, No. 1805978.
(14) Zhang, K.; Lee, T. H.; Bubach, B.; Jang, H. W.; Ostadhassan, M.; Choi, J.-W.; Shokouhimehr, M. Graphite carbon-encapsulated metal nanoparticles derived from Prussian blue analogs growing on natural loofa as cathode materials for rechargeable aluminum-ion batteries. *Sci. Rep.* **2019**, *9*, No. 13665.
(15) Zhang, K.; Lee, T. H.; Cha, J. H.; Jang, H. W.; Shokouhimehr, M.; Choi, J.-W. S@GO as a high-performance cathode material for rechargeable aluminum-ion batteries. *Electron. Mater. Lett.* **2019**, *15*, 720−726.
(16) Zhang, K.; Lee, T. H.; Cha, J. H.; Jang, H. W.; Shokouhimehr, M.; Choi, J.-W. Properties of CoS_2/CNT as a cathode material of rechargeable aluminum-ion batteries. *Electron. Mater. Lett.* **2019**, *15*, 727−732.
(17) Ma, L.; Chen, T.; Zhu, G.; Hu, Y.; Lu, H.; Chen, R.; Liang, J.; Tie, Z.; Jin, Z.; Liu, J. Pitaya-like microspheres derived from Prussian blue analogues as ultralong-life anodes for lithium storage. *J. Mater. Chem. A* **2016**, *4*, 15041−15048.
(18) Ma, L.; Chen, R.; Hu, Y.; Zhu, G.; Chen, T.; Lu, H.; Liang, J.; Tie, Z.; Jin, Z.; Liu, J. Hierarchical porous nitrogen-rich carbon nanospheres with high and durable capabilities for lithium and sodium storage. *Nanoscale* **2016**, *8*, 17911−17918.
(19) Sun, P.; Zhao, X.; Chen, R.; Chen, T.; Ma, L.; Fan, Q.; Lu, H.; Hu, Y.; Tie, Z.; Jin, Z.; Xu, Q.; Liu, J. $Li_3V_2(PO_4)_3$ encapsulated flexible free-standing nanofabric cathodes for fast charging and long life-cycle lithium-ion batteries. *Nanoscale* **2016**, *8*, 7408−7415.
(20) Lu, H.; Chen, R.; Hu, Y.; Wang, X.; Wang, Y.; Ma, L.; Zhu, G.; Chen, T.; Tie, Z.; Jin, Z.; Liu, J. Bottom-up synthesis of nitrogen-doped porous carbon scaffolds for lithium and sodium storage. *Nanoscale* **2017**, *9*, 1972−1977.
(21) Tabassum, H.; Zou, R.; Mahmood, A.; Liang, Z.; Wang, Q.; Zhang, H.; Gao, S.; Qu, C.; Guo, W.; Guo, S. A universal strategy for hollow metal oxide nanoparticles encapsulated into B/N Co-doped graphitic nanotubes as high-performance lithium-ion battery anodes. *Adv. Mater.* **2018**, *30*, No. 1705441.
(22) Xu, Q.; Sun, J.-K.; Yu, Z.-L.; Yin, Y.-X.; Xin, S.; Yu, S.-H.; Guo, Y.-G. SiO_x encapsulated in graphene bubble film: an ultrastable Li-ion battery anode. *Adv. Mater.* **2018**, *30*, No. 1707430.
(23) Xu, Q.; Sun, J. K.; Yin, Y. X.; Guo, Y.-G. Facile synthesis of blocky SiO_x/C with graphite-like structure for high-performance lithium-ion battery anodes. *Adv. Funct. Mater.* **2018**, *28*, No. 1705235.
(24) Cui, J.; Yao, S.; Lu, Z.; Huang, J.-Q.; Chong, W. G.; Ciucci, F.; Kim, J.-K. Revealing pseudocapacitive mechanisms of metal dichalcogenide SnS_2/graphene-CNT aerogels for high-energy Na hybrid capacitors. *Adv. Energy Mater.* **2018**, *8*, No. 1702488.
(25) Ock, I. W.; Choi, J. W.; Jeong, H. M.; Kang, J. K. Synthesis of pseudocapacitive polymer chain anode and subnanoscale metal oxide cathode for aqueous hybrid capacitors enabling high energy and power densities along with long cycle life. *Adv. Energy Mater.* **2018**, *8*, No. 1702895.
(26) Chen, J.; Yang, B.; Hou, H.; Li, H.; Liu, L.; Zhang, L.; Yan, X. Disordered, large interlayer spacing, and oxygen-rich carbon nanosheets for potassium ion hybrid capacitor. *Adv. Energy Mater.* **2019**, *9*, No. 1970069.
(27) Ding, J.; Wang, H.; Li, Z.; Cui, K.; Karpuzov, D.; Tan, X.; Kohandehghan, A.; Mitlin, D. Peanut shell hybrid sodium ion capacitor with extreme energy-power rivals lithium ion capacitors. *Energy Environ. Sci.* **2015**, *8*, 941−955.
(28) Chen, S.; Wang, J.; Fan, L.; Ma, R.; Zhang, E.; Liu, Q.; Lu, B. An ultrafast rechargeable hybrid sodium-based dual-ion capacitor based on hard carbon cathodes. *Adv. Energy Mater.* **2018**, *8*, No. 1800140.
(29) Zhang, K.; Lee, T. H.; Noh, H.; Islamoglu, T.; Farha, O. K.; Jang, H. W.; Choi, J.-W.; Shokouhimehr, M. Realization of lithium-ion capacitors with enhanced energy density via the use of gadolinium hexacyanocobaltate as a cathode material. *ACS Appl. Mater. Interfaces* **2019**, *11*, 31799−31805.
(30) Zhang, K.; Hong, K.; Suh, J. M.; Lee, T. H.; Kwon, O.; Shokouhimehr, M.; Jang, H. W. Facile synthesis of monodispersed Pd nanocatalysts decorated on graphene oxide for reduction of nitroaromatics in aqueous solution. *Res. Chem. Intermed.* **2019**, *45*, 599−611.
(31) Zhang, K.; Suh, J. M.; Choi, J.-W.; Jang, H. W.; Shokouhimehr, M.; Varma, R. S. Recent advances in the nanocatalyst-assisted $NaBH_4$ reduction of nitroaromatics in water. *ACS Omega* **2019**, *4*, 483−495.
(32) Zhang, K.; Suh, J. M.; Lee, T. H.; Cha, J. H.; Choi, J.-W.; Jang, H. W.; Varma, R. S.; Shokouhimehr, M. Copper oxide-graphene oxide nanocomposite: efficient catalyst for hydrogenation of nitroaromatics in water. *Nano Convergence* **2019**, *6*, No. 6.
(33) Yousaf, A. B.; Imran, M.; Farooq, M.; Kasak, P. Interfacial phenomenon and nanostructural enhancements in palladium loaded lanthanum hydroxide nanorods for heterogeneous catalytic applications. *Sci. Rep.* **2018**, *8*, No. 4354.
(34) Muthusankar, G.; Sethupathi, M.; Chen, S.-M.; Devi, R. K.; Vinoth, R.; Gopu, G.; Anandhan, N.; Sengottuvelan, N. N-doped carbon quantum dots@hexagonal porous copper oxide decorated multiwall carbon nanotubes: a hybrid composite material for an efficient ultra-sensitive determination of caffeic acid. *Composites, Part B* **2019**, *174*, No. 106973.
(35) Xiao, Q.; Feng, J.; Feng, M.; Li, J.; Liu, Y.; Wang, D.; Huang, S. A ratiometric electrochemical aptasensor for ultrasensitive determination of adenosine triphosphate via a triple-helix molecular switch. *Microchim. Acta* **2019**, *186*, No. 478.

DOI: 10.1021/acsomega.9b03699
ACS Omega 2020, 5, 1634−1639